Realtime measurement of phase partitioning of organic compounds using a Proton-Transfer-Reaction Time-of-Flight Mass Spectrometer coupled to a CHARON inlet

Yarong Peng[1,2], Hongli Wang[2,*], Yaqin Gao[2], Shengao Jing[2], Shuhui Zhu[2], Dandan Huang[2], Peizhi Hao[3], Shengrong Lou[2], Tiantao Cheng[4,5,*], Cheng Huang[2], Xuan Zhang[3,*]

[1] Department of Environmental Science and Engineering, Fudan University, Shanghai, 200438, China

[2] State Environmental Protection Key Laboratory of Formation and Prevention of Urban Air Pollution Complex, Shanghai Academy of Environmental Sciences, Shanghai, 200233, China

[3] School of Natural Sciences, University of California, Merced, 95343, USA

[4] Department of Atmospheric and Oceanic Sciences, Fudan University, Shanghai, 200438, China

[5] Big Data Institute for Carbon Emission and Environmental Pollution, Fudan University, Shanghai, 200438, China

Correspondence to: Hongli Wang (wanghl@saes.sh.cn), Tiantao Cheng (ttcheng@fudan.edu.cn), Xuan Zhang (xzhang87@ucmerced.edu)

Abstract. Understanding the gas-particle partitioning of semivolatile organic compounds (SVOCs) is of crucial importance in the accurate representation of the global budget of atmospheric organic aerosols. In this study, we quantified the gas- vs. particle-phase fractions of a large number of SVOCs in real time in an urban area of East China with the use of a CHemical Analysis of aeRosols ONline (CHARON) inlet coupled to a high resolution Proton Transfer Reaction Time-of-Flight Mass Spectrometer (PTR-ToF-MS). We demonstrated the use of the CHARON inlet for highly efficient collection of particulate SVOCs while maintaining the intact molecular structures of these compounds. The collected month-long dataset with hourly resolution allows us to examine the gas-particle partitioning of a variety of SVOCs under ambient conditions. By comparing the measurements with model predictions using the instantaneous equilibrium partitioning theory, we found that the dissociation of large parent molecules during the PTR ionization process likely introduces large uncertainties to the measured gas- vs. particle-phase fractions of less oxidized SVOCs, and therefore, caution should be taken when linking the molecular composition to the particle volatility when interpreting the PTR-ToF-MS data. Our analysis suggests that understanding the fragmentation mechanism of SVOCs and accounting for the neutral losses of small moieties during the molecular feature extraction from the raw PTR mass spectra could reduce, to a large extent, the uncertainties associated with the gas-particle partitioning measurement of SVOCs in the ambient atmosphere.

1. Introduction

Gas-particle partitioning of semivolatile organic compounds (SVOCs) is a critical process involved in the formation and evolution of atmospheric organic aerosols (OA). Traditionally,

41 gas-particle equilibrium partitioning of organic substances is assumed to be established

42 instantaneously (Zhang and Seinfeld, 2013), this assumption is in question if particles are semi-

43 solid or glassy (Shiraiwa et al., 2013). Most studies to date addressing the kinetic limitations in

44 partitioning have used indirect and/or theoretical methods that are lack of chemical and

45 molecular specificity (Mai et al., 2015; Shiraiwa and Seinfeld, 2012). Direct measurements of

46 gas-particle partitioning of SVOCs are needed in order to develop accurate parameterizations

47 for the organic aerosol formation in climate models.

48   The major challenge in the characterization of gas-particle partitioning of SVOCs lies in

49 the realtime measurement of labile compounds while maintaining their intact molecular

50 structures with minimal fragmentation (Zhang et al., 2016a; Zhang et al., 2016b; Zhang et al.,

51 2019). In recent years, soft ionization techniques coupled to mass spectrometry have been

52 widely used for the measurement of gas-phase SVOCs at the molecular level (Veres et al., 2008;

53 Crounse et al., 2006; Heald and Kroll, 2020). Combined with thermal desorption methods, these

54 techniques have also been deployed to measure organic compounds in both gas and particle

55 phases nearly simultaneously (Krechmer et al., 2016). A notable example would be the use of

56 the Filter Inlet for Gases and AEROsols coupled with the Chemical Ionization Mass

57 Spectrometry (FIGAERO-CIMS) to quantify the gas-particle partitioning of a broad range of

58 organic compounds in real time (Lopez-Hilfiker et al., 2014; Ye et al., 2021; Voliotis et al., 2021;

59 Wang et al., 2020a; Lutz et al., 2019; Lee et al., 2018; Le Breton et al., 2018; Stark et al., 2017;

60 Lopez-Hilfiker et al., 2016; Lopez-Hilfiker et al., 2015; Palm et al., 2020). A number of studies

61 among those have reached a consensus that the thermograms method, i.e., using the calibrated

62 thermal desorption profiles vs. temperature to derive the volatility, likely provides the best

63 estimates of the actual phase distribution. In contrast, using the directly measured gas- and

64   particle-phase fractions of a given analyte will most likely introduce a significant positive or

65   negative bias to the volatility estimation due to the thermal decomposition of labile organic

66   compounds during the desorption process (Lopez-Hilfiker et al., 2015; Stark et al., 2017). Such

67   thermal decomposition (or ion fragmentation) artifacts, either positive or negative depending

68   on the molecular size, have been suggested to constitute the largest uncertainties in the

69   estimation of phase partitioning behaviors of SVOCs using the thermal desorption method at

70   ambient pressure (Thompson et al., 2016).

71   Along with the line of thermal desorption method development, an inlet designed for the

72   CHemical Analysis of aeRosols ONline (CHARON) has been developed and coupled to the

73   Proton Transfer Reaction Time-of-Flight Mass Spectrometer (PTR-ToF-MS) in recent years.

74   As CHARON-PTR-ToF-MS does not rely on any form of pre-concentration on surfaces, it

75   could provide online and direct measurements of organic compounds in both phases, compared

76   with traditional thermal desorption instruments which still need to address artifacts during the

77   particle collection and desorption processes. Another potential advantage of CHARON-PTR-

78   ToF-MS is that the chemical information of the collected particles can be studied qualitatively

79   and quantitatively over a chemical composition level even at sub-nanogram mass

80   concentrations per molecule owing to the well studied ion-molecule reaction chemistry in PTR-

81   ToF-MS (Piel et al., 2019). CHARON has shown promising potential in the realtime analysis

82   of the chemical composition and spatiotemporal distributions of aerosols with laboratory-,

83   ground-, and aircraft-based platforms (Piel et al., 2019; Tan et al., 2018; Gkatzelis et al., 2018a;

84   Gkatzelis et al., 2018b; Muller et al., 2017; Eichler et al., 2017; Eichler et al., 2015; Antonsen

85   et al., 2017; Leglise et al., 2019; Piel et al., 2021). As a relatively new technique, the use of

86   CHARON-PTR-ToF-MS to investigate the gas-particle partitioning of organic compounds is

87 still quite limited. Only one study by Gkatzelis et al. (2018b) deployed CHARON, together

88 with two other aerosol sampling inlets, to measure the OA formation and aging from

89 monoterpenes and real plant emissions in chamber experiments. Whether the CHARON inlet

90 can be applied to the study of gas-particle partitioning of organic compounds under the actual

91 atmospheric conditions remains to be validated.

92   In this study, we assess the applicability of the CHARON inlet to the time-resolved

93 collection of organic compounds in their native molecular state using laboratory tests with a

94 series of authentic standards. We further employ the CHARON inlet coupled to a high

95 resolution PTR-ToF-MS instrument to measure an array of gaseous and particulate SVOCs in

96 an urban area of East China. The obtained month-long hourly dataset allows us to examine the

97 gas-particle partitioning of SVOCs spanning a range of volatilities. By comparing the

98 measurements with model predictions using the instantaneous equilibrium partitioning theory,

99 we found that fragmentation during the PTR ionization process may introduce large

100 uncertainties to the measured gas- vs. particle-phase fractions of less oxidized SVOCs.

101 Understanding the dissociation patterns of parent molecules and accounting for the

102 fragmentation losses when extracting the molecular features from the raw PTR mass spectra

103 are needed to improve the measured accuracy of SVOCs partitioning between the gas and

104 particle phase.

105

106 **2.   Material and Methods**

107 **2.1. Sampling site**

108   The sampling site located in the campus of the Shanghai Academy of Environmental

109 Science (SAES) is representative of a typical urban setting surrounded by restaurants, shopping

110   malls, and residential and commercial buildings (Fig. S1). Two traffic-heavy streets in the area

111   (Caobao Road and Humin Highway) are located ~ 150 m and 450 m lateral distances to the east

112   of the sampling site. A few number of petrochemical and chemical industrial facilities are

113   located ~ 50 km to the south and southwest of the observation site, which likely bring certain

114   long-lived pollutants to the site at a typical wind speed of ~ 1 – 3 m/s. Major pollution sources

115   in the area include traffic, commercial and residential activities, and regional transport (Huang

116   et al., 2021; Peng et al., 2023). The sampling inlet of the PTR-ToF-MS instrument was installed

117   on the roof of an eight-story building ~ 24 m above the ground. A comprehensive measurement

118   of gas- and particle-phase compounds in the ambient air was performed from Oct 24 to Nov 22.

119   During the sampling period, the average temperature, relative humidity, and wind speed were

120   18.0 ± 3.0 °C, 61.0 ± 15.0%, and 1.8 ± 0.7 m/s, respectively. The prevailing wind direction in

121   this region was from the northwest and north during the polluted period (Fig. S2).

122   **2.2. CHARON-PTR-ToF-MS**

123   **2.2.1.   Operation protocols**

124   A Proton Transfer Reaction Time-of-Flight Mass Spectrometer (PTR-ToF-MS) coupled to

125   a CHemical Analysis of aeRosols ONline (CHARON, Ionicon Analytik Inc, Innsbrunck,

126   Austria) inlet was employed to measure the gas- and particle-phase concentrations of a series

127   of SVOCs. The PTR-ToF-MS instrument used here is equipped with a radio frequency (RF)-

128   only quadrupole ion guide that transmits ions more efficiently (PTR-QiTOF, Ionicon Analytik

129   Inc) but results in a low-mass cutoff (Fig. S4). The operating parameters of the PTR-ToF-MS

130   were held constant during the entire measurement period. The drift tube pressure, temperature,

131   and voltage were 2.9 mbar, 120 °C, and 500 V, respectively. These conditions correspond to an

132   E/N (E is the electric field, and N is the number density of the gas molecules in the drift tube)

133 value of ~ 100 Td (1 Td = 10^{-17} V cm^2) and a reaction time of 120 μs. Note that the *E/N* value

134 determines the collision energy of ions in the reactor and therefore the degree of fragmentation

135 and cluster formation. The operating conditions were selected for the purpose of relatively low

136 fragmentation intensities (compared to 120 – 140 Td) and limited production of water clusters

137 (compared to 60 – 80 Td). Low *E/N* enhances the degree of water clustering, which complicates

138 the analysis of analyte ions due to a complex interplay between cluster formation ($RH^+(H_2O)_n$)

139 and proton transfer reactions (Holzinger et al., 2019). During the campaign, the sensitivity of

140 the PTR-ToF-MS was in the range of 300 – 1000 ncps ppb^{-1} and the mass resolution was

141 maintained at ~ 5000 m/Δm. Mass spectra were collected at a time resolution of 10 s.

142 The CHARON inlet consists of 1) a gas-phase denuder (GPD) for stripping off gas-phase

143 analytes, 2) an aerodynamic lens (ADL) for particle collimation which is combined with an

144 inertial sampler for emanating the particle-enriched flow, and 3) a thermo-desorption unit (TDU)

145 for particle volatilization. The CHARON inlet functionality has been described in great detail

146 by Eichler et al. (2015). The inlet we used here had a particle enrichment factor of ~ 15, as

147 discussed shortly. The vaporizer (TDU) was operated at 140 °C and ~ 8 mbar absolute pressure.

148 This temperature was chosen to ensure all the unknowns observed in the field can be evaporated

149 effectively while maintaining relatively intact molecular structures, see more details in Section

150 3.1. Measurements of organic compounds in the gas and particle phase were conducted using a

151 parallel sampling system with two independent pumps, allowing for the selection of flow rates

152 specifically adjusted for each phase, resulting in the overall residence time of less than 2 s (Fig.

153 S3).

154 **2.2.2. Sampling alternation between gas and particle phase**

155 Gas-phase compounds were measured by directly sampling the ambient air via a 2 m long

perfluoro-alkoxy (PFA) tube (1/4'' OD) capped with a polytetrafluoroethylene (PTFE) filter (Mitex[TM] PTFE membrane, 5 μm pore size, 47 mm diameter) to prevent the clogging of particles in the PTR capillaries. The gas-phase inlet was independently connected to the PTR-ToF-MS instrument upstream of the drift tube via a pressure-controlled subsampling PEEK capillary (1/16'' OD). Zero measurements were performed by overflowing catalytically (platinum at 370°C) purified air through the inlet. Ambient particles were sampled through a stainless steel tube (3/8'' OD) with a flow rate of ~ 3 L min^{-1}, out of which a flow of ~ 500 ml min^{-1} was directed to the CHARON inlet. A PM$_{2.5}$ cyclone was installed in front of the sampling line to remove coarse particles (> 2.5 μm). The particle-phase background was measured by placing a High-Efficiency Particulate Air filter (HEPA, HEPA-CAP 7, GE Healthcare UK Limited, Buckinghamshire, UK) upstream of the CHARON inlet. Servo motor activated valves made of passivated stainless steel were used for switching between the two inlet configurations. During the campaign, CHARON-PTR-ToF-MS automatically switched between gas and particle phase every 15 min. Detailed setup is given in Fig. S3 in the Supporting Information.

The built-in PTR-manager software (Ionicon Analytik GmbH, Innsbruck, Austria) offers the possibility to program sequences by which the instrument switches between different settings. It takes ~ 1 min for gases and particles to re-equilibrate when switching between these two modes. Data generated during this transition period (~ 2 min) were not considered. Instrument background was measured for 15 min every 5h. The limits of detection (LoD) at 1 min resolution were in the range of 5.6 ± 2.9 ng m^{-3} for gases and 0.7 ± 0.5 ng m^{-3} for particles, respectively (Fig. S5). Concentrations of gaseous and particulate compounds shown here included the last 5 min of every gas/particle-phase working mode, in order to minimize the interferences carried over from the previous working mode by allowing for a sufficient amount

179   of equilibration time in the inlet (Piel et al., 2021). In order to synchronize the gas- and particle-

180   phase data to calculate gas-particle partitioning, the average hourly data were then used for

181   further analysis.

182   **2.2.3.   Sensitivity and calibration**

183   Weekly calibrations were performed using a multicomponent calibration gas standard

184   (Linde, USA) at five concentration levels from 0.5 to 10 ppb (Fig. S4a). The calibration mixture

185   includes methanol, acetonitrile, acetaldehyde, acrolein, acetone, isoprene, methyl vinyl ketone,

186   methyl ethyl ketone, 2-pentanone, toluene, styrene, p-xylene, 1,3,5-trimethylbenzene,

187   naphthalene and α-pinene. Calibration standards with higher molecular weight were excluded

188   because we only considered ion masses below 200 amu from the field measurement for the

189   study of gas-particle partitioning, see discussions given in Text S1. Here the sensitivity of PTR-

190   ToF-MS is defined as the normalized ion intensity of RH^+ (ncps) obtained at a mixing ratio of

191   1 ppb. For a given species (R), its sensitivity (S, ncps ppb^{-1}) is a linear function of the rate

192   constant of its reaction with H_3O^+ (k) :

$$S = \frac{\frac{I_{RH^+}}{I_{H_3O^+}} \times 10^6}{\frac{[R]}{N} \times 10^9} = k \times N \times 10^{-3} \times t \times \frac{T_{RH^+}}{T_{H_3O^+}} \times F_{RH^+} \tag{1}$$

193

$$\text{corrected } S = \frac{S}{\frac{T_{RH^+}}{T_{H_3O^+}} \times F_{RH^+}} = a \times k \tag{2}$$

194

195   where the signals of H_3O^+ ($I_{H_3O^+}$) and RH^+ ions (I_{RH^+}) measured by the mass analyzer (in cps)

196   can be related to the signals of H_3O^+ ($[H_3O^+]$) and RH^+ ($[RH^+]$) ions at the end of the drift tube,

197   using their respective transmission efficiencies ($T_{H_3O^+}$ and T_{RH^+}) from the drift tube to the

198   detector (De Gouw and Warneke, 2007). $[R]$ is the concentration of species R and N is the

199   number density of gas in the drift tube. The reaction time (t) is determined by the ion drift

velocity. F_{RH^+} represents the fraction of product ions detected as RH^+ ions ($0 \leq F_{RH^+} \leq 1$). For non-fragmenting compounds, $F_{RH^+} = 1$. The measured sensitivity is further corrected by accounting for fragmentation and transmission efficiency, the value of which was derived from laboratory experiments (Fig. S4a). Uncertainties associated with the addition of the low-mass filter have been accounted for in the regression of individual transmission efficiency measurements on corresponding mass to charge ratios. The overall relative standard deviations were less than 15%. a is the slope of the linear regression of the corrected sensitivities on the proton-transfer-reaction rate coefficients (k), as shown in Fig. S4b. Following the method by Sekimoto et al. (2017), the linear regression result was used to determine the sensitivities of all uncalibrated species. The overall uncertainty was less than 15% for compounds with standards and around 50% for those without standards. Calculated sensitivity based on this method agrees well with measurements of authentic standards (Fig. S4c).

2.2.4. Enrichment factor

The CHARON inlet was calibrated routinely with pure ammonium nitrate particles to derive the enrichment factor as a function of the particle size following the procedures described in Eichler et al. (2015). In addition, we used a selection of authentic standards (Table S1) to test the effect of desorption temperature on the enrichment factor of labile compounds. Previous studies with CHARON generally used a temperature of 140 °C to vaporize particles (Leglise et al., 2019; Gkatzelis et al., 2018b; Tan et al., 2018). Herein, we tested the TDU temperature ranging from 70 to 140°C. The selected chemical standards were individually dissolved in distilled water (ethanol in the case of 2-Pentadecanone and 1-Pentadecanol) and nebulized by an atomizer (TSI 3076, Shore-view, MN, USA) that was pressurized with ultrapure zero air. The nebulizer outflow was diverted through two diffusion dryers to remove water vapor and an

223   activated charcoal denuder (NovaCarb F, Mast Carbon International Ltd., Guilford, UK) to

224   remove organic vapors. The resulting flow of polydisperse particles was then delivered into a

225   differential mobility analyzer (DMA, TSI 3080) for particle size selection. The transmitted

226   particles at a given size bin (300 nm for organics and $100 - 450$ nm range for ammonium nitrate)

227   were introduced into the CHARON-PTR-ToF-MS analyzer and a condensation particle counter

228   (CPC, TSI 3775), respectively. Particle mass concentrations were calculated based on the CPC

229   number distribution measurements by assuming a shape factor of 0.8 for ammonium nitrate

230   particles and 1 for organic particles, respectively.

231   The particle enrichment factor (*EF*) of a given analyte i was calculated as the ratio of the

232   PTR-ToF-MS derived vs. CPC derived mass concentrations of analyte i at a given particle size

233   bin:

234
$$VMR_{(PTR)i} = \frac{I_i}{S_i} \tag{3}$$

235
$$VMR_{(CPC)i} = \rho_i \times V \times N_i \times V_m / Mw_i \tag{4}$$

236
$$EF = \frac{VMR_{(PTR)i}}{VMR_{(CPC)i}} \tag{5}$$

237   where I_i is the normalized signal of species i (ncps) by PTR-ToF-MS, S_i is the sensitivity

238   (ncps ppb^{-1}), *VMR* is the volume mixing ratio (ppb), ρ is the density of species i (g cm^{-3}),

239   V is the volume of a particle sphere (m^3), N_i is the number concentration of particles measured

240   by CPC (cm^{-3}), V_m is the molar volume of an ideal gas at 1 atm (22.4 L mol^{-1}), Mw_i is the

241   molecular weight (g mol^{-1}). As the calculated sensitivities of most organics in the absence of

242   authentic standards are subject to uncertainties ($15\% - 50\%$), we will herein use the

243   multiplication of *EF* and S_i to evaluate the combined effect of CHARON enrichment and

244   sensitivity on the measured concentrations of a given analyte i in the particle phase.

2.2.5. Data processing

Data were analyzed using the Tofware package (v3.2.0, Tofwerk Inc), within the Igor Pro software (v7.0, Wavemetrics). Using this package, time-dependent mass calibrations were performed using four ions ($H_3^{18}O^+$, NO^+, $C_6H_5I^+$ and $C_6H_5I_2^+$), where $C_6H_5I^+$ and $C_6H_5I_2^+$ were produced from the internal standard di-iodobenzene. The relative mass deviation was within 6 − 8 ppm across the mass spectra. Considering the humidity dependence of reagent ions (H_3O^+ and $H_3O^+(H_2O)$), the fitted product ion signals (RH^+) were normalized to a standard reagent ion of 10^6 cps (counts per second). Elemental composition was determined based on the accurate *m/z* (mass to charge ratio) and isotopic pattern analysis. A list of ~ 1600 ions was extracted, including both gas- and particle-phase ions. Molecular formulas including only C, H, and O atoms were assigned to the detected ions by the addition of one proton in cases where the elemental composition analysis returned multiple options. About 85% of the signals were elementally resolved by the $C_xH_yO_z$ formula in ambient air mass spectra. A small number of nitrogen containing compounds, such as nitroaromatics, were also identified but not included in the following analysis. Throughout of the context, we use the word "species" to refer to all compounds with assigned molecular formula, which may include multiple isomers.

2.3. Complementary measurements

In addition to CHARON-PTR-ToF-MS, a Thermal desorption Aerosol Gas chromatograph (TAG) was also employed to measure a series of particle-phase organic species. Details of the TAG operation and data analysis protocols can be found in previous studies (He et al., 2020; Wang et al., 2020b; Zhu et al., 2021). The elemental composition and mass concentration of particles were measured by an Aerodyne high-resolution time-of-flight Aerosol Mass Spectrometer (AMS), with details of operation and quality control protocols given by our recent

268   study (Huang et al., 2021). Volatile organic compounds (VOCs, $C_2 - C_{12}$) were analyzed by a

269   custom-built online gas chromatography system equipped with a mass spectrometer and a flame

270   ionization detector (GC-MS/FID). The performance of this system can be found in our previous

271   publications (Zhu et al., 2018; Wang et al., 2014). Meteorological parameters (ambient

272   temperature, wind speed, wind direction, and relative humidity) were collected by an automatic

273   weather station (Metone 590 series) mounted on the roof top of the campaign site.

274   **2.4. Gas-particle partitioning measurements vs. modeling**

275   The CHARON-PTR-ToF-MS measured gas- and particle-phase concentrations of a given

276   species i can be used to calculate its particle-phase fraction ($F_{p,i}$).

277
$$P_i = \frac{\frac{I_{p,i} \times \left(\frac{m}{z_i} - 1\right)}{V_m \times S_i}}{EF} \tag{6}$$

278
$$G_i = \frac{I_{g,i} \times \left(\frac{m}{z_i} - 1\right)}{V_m \times S_i} \tag{7}$$

279
$$F_{p,i} = \frac{P_i}{P_i + G_i} \tag{8}$$

280   where P_i and G_i are the mass concentrations (ng m^{-3}) of species i in the particle and gas

281   phase, respectively. $I_{p,i}$ and $I_{g,i}$ are the normalized signal (ncps) of the PTR-ToF-MS detected

282   ion i in the particle and gas phase, respectively. V_m is taken as 22.4 L/mol. S_i is calculated

283   or measured sensitivity (ncps ppb^{-1}), see details in Section 2.2.3. As structural isomers cannot

284   be resolved in the mass spectra, the calculation here assumes that all isomers with the same

285   molecular formula have the same chemical properties, i.e., saturation vapor pressures.

286   Substitution of Equations (6) and (7) to Equation (8) yields the final expression of the particle-

287   phase fraction of species i ($F_{p,i}$), which is a function of the observed PTR-MS raw signals of

288   species i in the gas and particle phase (in total ion counts), as well as the particle enrichment

289   factor (EF) of species i.

$$F_{p,i} = \frac{I_{p,i}/EF}{I_{p,i}/EF + I_{g,i}} \tag{9}$$

291   Gas-particle partitioning of a given analyte i was also modeled using the equilibrium

292   partitioning theory (Pankow, 1994):

$$F_{p,i} = \frac{1}{1 + C_i^* / C_{OA}} \tag{10}$$

$$C_i^* = \frac{10^6 Mw_i \zeta_i p_i}{RT} \tag{11}$$

295   where C_{OA} is the organic aerosol concentration measured by AMS (μg m^{-3}), C_i^* is the

296   saturation mass concentration (μg m^{-3}), Mw_i is the molecular weight (g mol^{-1}), ζ is the

297   activity coefficient (assumed as unity), p_i is the pure component liquid vapor pressure (Pa), R

298   is the universal gas constant (8.2×10^{-5} m^3 atm K^{-1} mol^{-1}), and T is the ambient temperature

299   (K). As detailed chemical information is lacking for all species detected by PTR-ToF-MS, here

300   we use the expression given by Donahue et al. (2011) to approximate the value of C_i^*:

$$\log_{10} C_i^* = \left(n_C^0 - n_C^i\right) b_C - n_O^i b_O - 2 \frac{n_C^i n_O^i}{n_C^i + n_O^i} b_{CO} \tag{12}$$

302   where $n_C^0 = 25$, $b_C = 0.475$, $b_O = 2.3$, and $b_{CO} = -0.3$.

2.5. Uncertainties in the measured and modeled gas-particle partitioning

304   The uncertainty associated with the PTR-MS measured concentrations in both gas and

305   particle phases is less than 15% for compounds with chemical standards based on the optimally

306   fitted transmission efficiency curve. For those in the absence of standards, their PTR

307   sensitivities were calculated theoretically using Equations (1-2), and the uncertainty in the

308   calculation mainly arises from the estimation of polarizability and dipole moment of the target

309   molecule, which has been estimated to be within ~ 50% when only the elemental composition

310   of that molecule is given (Sekimoto et al., 2017). It is important to note, however, that the

311   uncertainty associated with the estimated PTR sensitivity has zero influence on the measured

312   particle-phase fraction of any given compound because the sensitivity term is essentially

313   canceled in the divisor function in Equation (9). The uncertainty associated with the particle

314   fraction of a given species i derived from the PTR-MS measurements arises predominantly

315   from the "EF" term. Since the uncertainty of the measured EF depends on the uncertainty of

316      $I_{p,i}$, we thus express the overall uncertainties of the measured gas-particle partitioning as:

317 $$Unc(F_{p,i}) = \sqrt{Unc(EF)^2 + Unc(I_{g,i})^2} \qquad (13)$$

318   with the calibration standards used in this study, the enrichment factor is calculated to be within

319   25% error ($Unc(EF)$) (see detailed calculations listed in Table S2 and S3), including the effect

320   of wall loss inside the inlet tubing and the precision of the measurement. Huang et al. (2019)

321   has tested the uncertainty of wall loss ($Unc(I_{g,i})$) in this PTR-MS instrument as 28%. Therefore,

322   the overall uncertainty in the measured particle-phase fraction ($Unc(F_{p,i})$) was estimated as

323   38%.

324   The uncertainty associated with the modeled gas-particle partitioning arises primarily from

325   the uncertainty in the estimation of the saturation mass concentration (C_i^*) based on the method

326   developed by Donahue et al. (2011). In this method, the saturation mass concentration of

327   species i is a non-linear function of the numbers of carbon and oxygen atoms in that particular

328   species, see Equation (12). For each generic molecular formula, i.e., C_xH_y, C_xH_yO, $C_xH_yO_2$, and

329      $C_xH_yO_4$, Donahue et al. (2011) have used a total of 25, 48, 18, and 10 chemical standards with

330   known volatilities to validate the estimated saturation concentrations, and the estimated errors

331   were taken as 34%, 16%, 25%, and 54%, respectively (see Table S6). As the $C_xH_yO_3$ group was

332 not tested, we tentatively assumed the associated errors as the same as the $C_xH_yO_4$ group. The

333 extent to which these uncertainties may affect the difference between measurements and model

334 results was discussed in detail in the Supporting Information (Fig. S10).

335

336 **3. Results and Discussion**

337 **3.1. Particle enrichment: effect of desorption temperature**

338   Thermal desorption as a common procedure used in the chemical characterization of

339 organic aerosols is often susceptible to fragmentation of non-refractory compounds. Due to the

340 high temperature used to evaporate particles collected, labile and large molecules are inevitably

341 subject to fragmentation, thereby introducing large uncertainties to the measured mass and

342 composition of the particulate organic compounds (Lopez-Hilfiker et al., 2015; Yatavelli et al.,

343 2012; Zhao et al., 2013). Thermal decomposition of oxidized organic compounds has been

344 observed at vaporizer temperature as low as 200 °C, the lowest temperature required to vaporize

345 OA as reported (Stark et al., 2017). While decreasing the vaporizer temperature is necessary to

346 maintain the intact structure of labile molecules, low temperature (e.g., 85 °C), however, might

347 fail to completely evaporate the collected particles into vapors, resulting in an underestimation

348 of the collected OA mass (Inomata et al., 2014). Here we performed a series of sensitivity tests

349 to identify the optimal vaporizer temperature in the CHARON inlet for the measurements of

350 organic compounds in the particle phase.

351   Prior to the temperature sensitivity test, we have validated that the particle enrichment

352 factor, also known as collection efficiency and defined as the ratio of the particle mass

353 concentration upstream to downstream of the aerodynamic lens, does not depend on the particle

354 size. As shown in Fig. 1a, the measured *EF* value for ammonium nitrate particles, detected as

355 NO_2^+ produced from the nitric acid vapor, remains constant as ~ 15 in the $150 - 450$ nm particle

356 size range. The lower values in the $100 - 150$ nm size range can be explained by the lower

357 particle transmission efficiency in the gas phase denuder, e.g., $75\% - 80\%$ for 100 nm particles

358 (Eichler et al., 2015). Also, particles below 150 nm are less efficiently concentrated in the

359 subsampling flow after the aerodynamic lens. Therefore, we used the monodisperse particles

360 generated from selected organic standards at 300 nm for the temperature sensitivity test.

361   A number of chemical standards that are representative of alcohols, carbonyls, and

362 carboxylic acids and with the vapor pressure ranging from 10^{-14} to 10^{-1} Pa at 25 °C (taken from

363 EPA EPI Suite (2012), see values given in Table S1) were used to generate organic aerosols,

364 which, upon size selection at 300 nm, were directed to the CHARON inlet. Particle evaporation

365 occurs downstream of the aerodynamic lens in the gas phase and on the tube and orifice surface

366 to which submicron particles rapidly diffuse at ~ 8 mbar operating pressure. The thermal

367 desorption unit was designed to ensure that ammonium sulfate particles (10^{-20} Pa) can be

368 completely evaporated (Piel et al., 2019; Eichler et al., 2015). As the desorption temperature

369 was varied from 70 °C to 140 °C, the intensities of all detected ions (including both parent and

370 fragment ions) for each organic standard analyzed were stable within 15%, as shown in Fig. 1b.

371 Also note that we did not observe any ions produced from decarboxylation and/or dehydration

372 during the particle evaporation process. This is because the relative low operation temperature

373 and the short heat exposure time could effectively limit any thermal dissociation of organic

374 molecules. This demonstrates that the parent molecule fragmentation, if any, does not occur

375 under the range of desorption temperature used in the CHARON inlet, but rather results from

376 the ionic dissociation process in the PTR ionization chamber, see more discussions in Section

377 3.3. We therefore used the sum total of intensities of all major ions detected as the PTR-ToF-

378 MS response to a given organic standard analyzed. Fig. 1c shows that the derived enrichment

379 factors stay constant for all compounds investigated ($Mw \sim 160 - 230$ g/mol). The relative

380 signals of all fragment ions were stable over the range of the desorption temperature as shown

381 in Fig. 2. This suggests that the desorption temperature used here, even as low as 70 °C, is

382 sufficient to evaporate SVOCs (volatility $> 10^{-14}$ Pa at 25 °C), due to the low operating pressure

383 (~ 8 mbar) that significantly enhances the partitioning shift to the gas phase. One low volatility

384 compound, sucrose (Mw is 342 g/mol and vapor pressure is 4.69×10^{-14} Pa), has a slightly lower

385 enhancement factor compared with all the other organic standards tested. This is mainly due to

386 the intensive dehydration of the parent compound in the ionization chamber, and as a result,

387 only a few fragment ions were captured, resulting in a lower PTR response and thereby lower

388 EF value calculated from Equations (3-5). The EF values of sucrose also have much higher

389 standard deviations at all temperatures due to fragmentation (Table S3).

390   It has been recognized that species with one functional group follow certain fragmentation

391 patterns during the PTR ionization process (Pagonis et al., 2019; Francis et al., 2007; Spanel et

392 al., 1997; Tani et al., 2003; Spanel and Smith, 1997), such as dehydration of acids and alcohols.

393 The observed dissociation of carboxylic acid standards used in this study, e.g., phthalic acid

394 and 3-methylbutane-1,2,3-tricarboxylic acid, can be explained by this common fragmentation

395 pattern. The fragmentation mechanism of muti-functionalized species is rather complicated and

396 a number of fragments can be produced upon PTR ionization. Nevertheless, the identity and

397 abundance of fragments from a given muti-functionalized species have been found comparable

398 under the same PTR operation protocols (Leglise et al., 2019; Gkatzelis et al., 2018a). For

399 example, *cis*-pinonic acid yields the following fragments (main ions only and relative

400 abundance in parentheses): *m/z* 71.049 (~28%), 115.075 (~36%), 167.108 (~19%), and 185.117

401 (~11%), which is comparable with an earlier study (Leglise et al., 2019): m/z 71.049 (~27%),

402 115.075 (~33%), 167.108 (~26%), and 185.117 (~14%) at 100 Td settings.

3.2. Molecular features of detected organic species

404   A month-long field dataset of particle- and gas-phase organic species was collected at

405 hourly resolution using the CHARON-PTR-ToF-MS instrument. A comparison of PTR-ToF-

406 MS measurements with other techniques available on site was performed for both gas and

407 particle phases. For the gas phase, quantitative measurements of a suite of VOCs by GC-

408 MS/FID, including benzene, toluene, styrene, C_8 and C_9 aromatics, acrolein, and C_4, C_5, and C_6

409 ketones, agree well with corresponding PTR-ToF-MS measurements, as shown in Fig. S6. For

410 the particle phase, the time series of a group of $C_xH_yO_4$ species (including $C_4H_6O_4$, $C_5H_8O_4$,

411 $C_6H_{10}O_4$, and $C_8H_6O_4$) are in reasonable agreement with corresponding measurements taken by

412 TAG (r ~ 0.60 – 0.80), although the CHARON-PTR-ToF-MS measured total molecular mass

413 is generally lower than the TAG measurements by a factor of 2 to 6 (Fig. S7). This is likely

414 caused by the fragmentation (e.g., loss of H_2O, see Fig. S8) of the parent compounds during the

415 ionization process, as discussed in detail in Section 3.3. The time series of total OA mass

416 characterized by CHARON-PTR-ToF-MS also agree with the AMS measurements (r ~ 0.91,

417 Fig. S9). Previous studies have reported the particulate organics measured by PTR-MS with a

418 thermal desorption inlect account for 25% – 60% mass of the total organic aerosols measured

419 by AMS (Holzinger et al., 2013). Direct comparison of the total OA mass loading is not

420 applicable here since the CHARON-PTR-ToF-MS measurement only focused on compounds

421 with the mass to charge ratio below 300 Th. That the majority of ions detected by PTR are

422 present in the lower mass range is primarily due to the fragmentation of larger masses during

423 the ionization process, as discussed extensively in Section 3.3.

424   Fig. 3 (a-b) shows the PTR-ToF-MS spectra of dominant ions averaged over the entire

425   campaign in both gas and particle phases. The mass concentrations of individual ions are in the

426   range of 7.9 – 7179.3 ng m^{-3} in the gas phase and 0.6 – 82.7 ng m^{-3} in the particle phase. A total

427   of 152 species (with > 60% data points above the PTR-ToF-MS detection limits) are identified,

428   contributing to ~ 69% and ~ 44%, respectively, of the total organic mass measured in the gas

429   and particle phase. The molecular distribution characterized by the carbon and oxygen of these

430   species is given in Fig. 3 (c-d). The most abundant species are characterized by a generic

431   formula of C_xH_yO and $C_xH_yO_2$, resolving ~ 64% and ~ 46% in total of all identified species in

432   the gas and particle phase, respectively. Another dominant component in the gas phase is

433   hydrocarbon-like compounds (C_xH_y) (~ 27%), which contribute ~ 12% of the organic mass in

434   the particle phase. Species with higher oxygen numbers (> 2) contribute to a large fraction (~

435   42%) of the total particulate mass. These $C_xH_yO_{1-4}$ groups exhibit different diurnal cycles, as

436   shown in Fig. 4, reflecting their unique formation chemistry. The C_xH_y group peaks in the early

437   morning rush hour and likely originates from primary traffic emissions. On the contrary, both

438    $C_xH_yO_3$ and $C_xH_yO_4$ groups peak at noon, suggesting a strong secondary formation source. The

439   diurnal trends for C_xH_yO and $C_xH_yO_2$ groups are relatively flat during the day, likely indicative

440   of an intertwined primary emission and secondary formation processes.

441   **3.3. Measured vs. modeled gas-particle partitioning**

442   Fig. 5 shows the calculated particle-phase fraction (F_p) of the identified 152 species using

443   the CHARON-PTR-ToF-MS measurements in both phases. It is important to note that an

444   authentic standard is not required for the calculation of F_p for any given species, because the

445   PTR sensitivity term is essentially canceled in the divisor function in Equations (6-8). Also

446   given in Fig. 5 is the simulated F_p of the derived molecular formulas of all species identified

447   using the equilibrium partitioning theory, see method described in Section 2.4. Interestingly,

448   for oxidized species such as $C_xH_yO_4$, their measured F_p agree reasonably with the simulations,

449   as shown in Fig. 5a. The $C_xH_yO_4$ group resides in the relatively higher mass range, and species

450   identified in this group are more likely actual compounds rather than fragments from larger

451   parent molecules. Even these species dessociate into lower mass ions during PTR ionization,

452   their calculated particle-phase fractions are unaffected by such fragmentation processes because

453   signals of parent ions decrease by the same extent upon fragmentation in both gas and particle

454   phases. As the oxygen number decreases, the measured F_p values tend to deviate from the

455   simulations by up to several orders of magnitude. Note that these less oxidized compounds (e.g.,

456   C_xH_y) are mostly small molecules and they are highly unlikely present in the condensed phase

457   as closed-shell monomers (Pankow and Asher, 2008; Holzinger et al., 2010). Instead, they are

458   more likely fragments produced from the decomposition of larger molecules, which no

459   surprisingly favor partitioning in the particle phase. It is worth noting that the uptake of small

460   oxidized compounds on the aerosol aqueous phase does not significantly affect the overall

461   particle phase fraction of these compounds, see detailed calculations in Text S3. The

462   discrepancy in the measurement-model comparison underscores the importance of

463   understanding the fragmentation mechanism during PTR ionization when extracting molecular

464   features from the raw mass spectra.

465   Parent ion fragmentation has been widely observed in PTR-MS instruments (Pagonis et al.,

466   2019). Oxygenates exhibit trends in neutral losses of water or saturated alcohols. Here, we

467   apply a correction to the molecular formula of the 152 identified species by assuming that these

468   species are fragments produced from their parent precursors through the neutral losses of a

469   carboxyl group ($-CO_2$), a carbonyl group ($-CO$), a hydroxyl group ($-H_2O$), or an alcohol group

470 (-C_2H_6O). By applying this correction, the modeled F_p of a given species $C_xH_yO_z$ would actually

471 represent the particle-phase fraction of the its parent species $C_xH_yO_z \cdot CO_2$, $C_xH_yO_z \cdot CO$,

472 $C_xH_yO_z \cdot H_2O$, or $C_xH_yO_z \cdot C_2H_6O$. As shown in Fig. 5 (b-e), such a correction could significantly

473 increase the modeled F_p values by several orders of magnitude. The assumption of neutral

474 losses of CO_2 or C_2H_6O allows for much improved agreement between modeled vs. measured

475 F_p values for less oxidized species. This implies that these small and less oxidized species are

476 likely fragments resulting from the decomposition of larger parent precursors. As our particle

477 enrichment test (details given in Section 3.1) has confirmed that the thermal desorption

478 temperature employed for particle evaporation does not lead to any intensive fragmentation,

479 therefore the collision-induced dissociation during the proton transfer reaction process becomes

480 the predominant process that produces fragments (Lindinger et al., 1998; Gueneron et al., 2015;

481 Gkatzelis et al., 2018b). Although the electric field applied to the drift tube is considered low

482 to moderate compared with most previous PTR-MS measurements ($E/N \sim 100$ Td in this study

483 vs. $E/N \sim 120 - 140$ Td commonly found in PTR-MS measurements) (Pagonis et al., 2019),

484 parent ion fragmentation was still widely observed here and complicated the mass spectra

485 interpretation and molecular feature extraction. While some recent CHARON measurements

486 employed lower electric field in the drift tube ($E/N \sim 60$ Td) (Leglise et al., 2019; Gkatzelis et

487 al., 2018a; Piel et al., 2019), such conditions could promote the formation of water cluster ions,

488 which increase with humidity and reduce the PTR sensitivity, and therefore are not ideally

489 suitable for our field measurements. A compromise solution would be using a moderate electric

490 field in the drift tube (e.g., ~ 100 Td) and meanwhile applying appropriate molecular corrections

491 to all ions detected in the mass spectra by considering possible neutral losses of small moieties.

492 Since in this study only the information of molecular formula is derived from the PTR-MS

493   spectra, we thus provide the lower and upper bound of the gas-particle partitioning corrections

494   owing to neutral losses of H_2O and CO_2, respectively. In general, lower masses with higher

495   volatilities are subject to notable changes in the particle-phase fraction as a result of neutral

496   losses during the PTR ionization process, see detailed discussions in Text S2.

497

4. Conclusions

499   Recent studies have suggested that some of the model-measurement discrepancies in the

500   representation of ambient organic aerosol budget might be due to the nonequilibrium

501   gas/particle partitioning caused by kinetic limitations in the presence of glassy or semi-solid

502   phase (Perraud et al., 2012; Mai et al., 2015; Shiraiwa et al., 2013). It is therefore necessary to

503   validate whether the equilibrium partitioning theory could adequately describe the

504   condensation of semivolatile organic vapors onto atmospheric aerosols under ambient

505   conditions, and the accurate measurement of these SVOCs in both gas and particle phases is

506   the crucial prerequisite. In this study, we have employed the PTR-ToF-MS instrument coupled

507   to a CHARON inlet, together with a suite of complementary measurements, to characterize the

508   atmospheric partitioning behaviors of an array of SVOCs in an urban environment of East

509   China. Prior to the application to the field measurements, we first performed a series of

510   laboratory experiments to test whether the CHARON inlet is capable of sampling organic

511   molecules (including alcohols, carbonyls, and carboxylic acids) in their native states. With the

512   low pressure condition used in the CHARON inlet, a thermal desorption temperature less than

513   140 °C could adequately evaporate organic compounds with vapor pressure higher than 10^{-14}

514   Pa while minimizing the thermal decomposition of labile functionalities. The auto-switch

515   function between the gas and particle mode with one single PTR-ToF-MS instrument could

516 monitor gaseous and particulate organic compounds in real time, thereby providing important

517 information of their partitioning behaviors in the ambient atmosphere. Particle-phase fractions

518 of a total of 152 organic species were derived from the CHARON-PTR-ToF-MS measurements

519 and further compared with model predictions using the instantaneous equilibrium partitioning

520 theory. While the model captured the particle-phase fraction of oxidized compounds (e.g.,

521 $C_xH_yO_{3-4}$), predictions of less oxidized compounds, notably the C_xH_y family, differ from the

522 corresponding measurements by several orders of magnitude. Such a large discrepancy is very

523 likely caused by the intensive fragmentation of the parent organic compounds during the PTR

524 ionization process. Accounting for common fragmentation patterns in the simulations of gas-

525 particle partitioning, for example, neutral losses of $-CO_2$, $-CO$, $-H_2O$, or $-C_2H_6O$, could largely

526 improve the model-measurement agreement. Such corrections are very necessary towards an

527 accurate measurement of both particle- and gas-phase SVOCs using the CHARON-PTR-ToF-

528 MS instrument. Our study suggests the crucial importance of optimizing operation conditions

529 and understanding the fragmentation mechanism in the particle collection, vaporization, and

530 ionization processes in understanding the gas-particle partitioning of organic compounds using

531 any thermal desorption based aerosol measurement method.

532

533 *Data availability.* The data shown in the paper are available upon request from the

534 corresponding author.

535 *Author Contributions.* YP carried out experiments and measurements and drafted the

536 manuscript. HW and XZ designed the experimental studies, supervised the laboratory work and

537 wrote the manuscript. YG and SJ supported the ambient measurements. SZ, DH, PH, and SL

538 supported the data analysis. TC and CH supervised the scientific work. All authors have given

539   approval to the final version of the manuscript.

540   *Competing interests.* The authors declare no competing financial interest.

541   *Acknowledgements.* This research has been supported by the National Natural Science

542   Foundation of China (No. 42175135, No. 42175179), the National Key R&D Programm of

543   China (No. 2022YFE0136200) and the Shanghai Science and Technology Commission of the

544   Shanghai Municipality (No. 20ZR1447800).

545

546   **References**

547   Antonsen, S., Bunkan, A. J. C., D'Anna, B., Eichler, P., Farren, N., Hallquist, M., Hamilton, J.
548   F., Kvarnliden, H., Mikoviny, T., Muller, M., Nielsen, C. J., Stenstrom, Y., Tan, W., Wisthaler,
549   A., and Zhu, L.: Atmospheric chemistry of tert-butylamine and AMP, in: Enrgy Proced, edited
550   by: Dixon, T., Laloui, L., and Twinning, S., Energy Procedia, Elsevier Science Bv, Amsterdam,
551   1026-1032, 10.1016/j.egypro.2017.03.1248, 2017.

552   Crounse, J. D., McKinney, K. A., Kwan, A. J., and Wennberg, P. O.: Measurement of gas-phase
553   hydroperoxides by chemical ionization mass spectrometry, Anal. Chem., 78, 6726-6732,
554   10.1021/ac0604235, 2006.

555   de Gouw, J. and Warneke, C.: Measurements of volatile organic compounds in the earths
556   atmosphere using proton-transfer-reaction mass spectrometry, Mass Spectrometry Reviews, 26,
557   223-257, 10.1002/mas.20119, 2007.

558   Donahue, N. M., Epstein, S. A., Pandis, S. N., and Robinson, A. L.: A two-dimensional
559   volatility basis set: 1. organic-aerosol mixing thermodynamics, Atmos. Chem. Phys., 11, 3303-
560   3318, 10.5194/acp-11-3303-2011, 2011.

561   Eichler, P., Muller, M., D'Anna, B., and Wisthaler, A.: A novel inlet system for online chemical
562   analysis of semi-volatile submicron particulate matter, Atmos. Meas. Tech., 8, 1353-1360,
563   10.5194/amt-8-1353-2015, 2015.

564   Eichler, P., Muller, M., Rohmann, C., Stengel, B., Orasche, J., Zimmermann, R., and Wisthaler,
565   A.: Lubricating Oil as a Major Constituent of Ship Exhaust Particles, Environ. Sci. Technol.

Lett., 4, 54-58, 10.1021/acs.estlett.6b00488, 2017.

EPA: Estimation Program Interface (EPI) Suite (v4.11), US [code], 2012.

Francis, G. J., Milligan, D. B., and McEwan, M. J.: Gas-Phase Reactions and Rearrangements of Alkyl Esters with H3O+, NO+, and O2•+: A Selected Ion Flow Tube Study, J. Phys. Chem. A, 111, 9670-9679, 10.1021/jp0731304, 2007.

Gkatzelis, G. I., Tillmann, R., Hohaus, T., Muller, M., Eichler, P., Xu, K. M., Schlag, P., Schmitt, S. H., Wegener, R., Kaminski, M., Holzinger, R., Wisthaler, A., and Kiendler-Scharr, A.: Comparison of three aerosol chemical characterization techniques utilizing PTR-ToF-MS: a study on freshly formed and aged biogenic SOA, Atmos. Meas. Tech., 11, 1481-1500, 2018a.

Gkatzelis, G. I., Hohaus, T., Tillmann, R., Gensch, I., Muller, M., Eichler, P., Xu, K. M., Schlag, P., Schmitt, S. H., Yu, Z. J., Wegener, R., Kaminski, M., Holzinger, R., Wisthaler, A., and Kiendler-Scharr, A.: Gas-to-particle partitioning of major biogenic oxidation products: a study on freshly formed and aged biogenic SOA, Atmos. Chem. Phys., 18, 12969-12989, 10.5194/acp-18-12969-2018, 2018b.

Gueneron, M., Erickson, M. H., VanderSchelden, G. S., and Jobson, B. T.: PTR-MS fragmentation patterns of gasoline hydrocarbons, International Journal of Mass Spectrometry, 379, 97-109, 10.1016/j.ijms.2015.01.001, 2015.

He, X., Wang, Q., Huang, X. H. H., Huang, D. D., Zhou, M., Qiao, L., Zhu, S., Ma, Y.-g., Wang, H.-l., Li, L., Huang, C., Xu, W., Worsnop, D. R., Goldstein, A. H., and Yu, J. Z.: Hourly measurements of organic molecular markers in urban Shanghai, China: Observation of enhanced formation of secondary organic aerosol during particulate matter episodic periods, Atmos. Environ., 240, 10.1016/j.atmosenv.2020.117807, 2020.

Heald, C. L. and Kroll, J. H.: The fuel of atmospheric chemistry: Toward a complete description of reactive organic carbon, Sci. Adv., 6, 10.1126/sciadv.aay8967, 2020.

Holzinger, R., Goldstein, A. H., Hayes, P. L., Jimenez, J. L., and Timkovsky, J.: Chemical evolution of organic aerosol in Los Angeles during the CalNex 2010 study, Atmos. Chem. Phys., 13, 10125-10141, 10.5194/acp-13-10125-2013, 2013.

Holzinger, R., Williams, J., Herrmann, F., Lelieveld, J., Donahue, N. M., and Rockmann, T.: Aerosol analysis using a Thermal-Desorption Proton-Transfer-Reaction Mass Spectrometer

(TD-PTR-MS): a new approach to study processing of organic aerosols, Atmos. Chem. Phys., 10, 2257-2267, 10.5194/acp-10-2257-2010, 2010.

Holzinger, R., Acton, W. J. F., Bloss, W. J., Breitenlechner, M., Crilley, L. R., Dusanter, S., Gonin, M., Gros, V., Keutsch, F. N., Kiendler-Scharr, A., Kramer, L. J., Krechmer, J. E., Languille, B., Locoge, N., Lopez-Hilfiker, F., Materić, D., Moreno, S., Nemitz, E., Quéléver, L. L. J., Sarda Esteve, R., Sauvage, S., Schallhart, S., Sommariva, R., Tillmann, R., Wedel, S., Worton, D. R., Xu, K., and Zaytsev, A.: Validity and limitations of simple reaction kinetics to calculate concentrations of organic compounds from ion counts in PTR-MS, Atmos. Meas. Tech., 12, 6193-6208, 10.5194/amt-12-6193-2019, 2019.

Huang, D. D., Zhu, S., An, J., Wang, Q., Qiao, L., Zhou, M., He, X., Ma, Y., Sun, Y., Huang, C., Yu, J. Z., and Zhang, Q.: Comparative Assessment of Cooking Emission Contributions to Urban Organic Aerosol Using Online Molecular Tracers and Aerosol Mass Spectrometry Measurements, Environ. Sci. Technol., 10.1021/acs.est.1c03280, 2021.

Huang, G., Liu, Y., Shao, M., Li, Y., Chen, Q., Zheng, Y., Wu, Z., Liu, Y., Wu, Y., Hu, M., Li, X., Lu, S., Wang, C., Liu, J., Zheng, M., and Zhu, T.: Potentially Important Contribution of Gas-Phase Oxidation of Naphthalene and Methylnaphthalene to Secondary Organic Aerosol during Haze Events in Beijing, Environ. Sci. Technol., 53, 1235-1244, 10.1021/acs.est.8b04523, 2019.

Inomata, S., Sato, K., Hirokawa, J., Sakamoto, Y., Tanimoto, H., Okumura, M., Tohno, S., and Imamura, T.: Analysis of secondary organic aerosols from ozonolysis of isoprene by proton transfer reaction mass spectrometry, Atmos. Environ., 97, 397-405, 10.1016/j.atmosenv.2014.03.045, 2014.

Krechmer, J. E., Groessl, M., Zhang, X., Junninen, H., Massoli, P., Lambe, A. T., Kimmel, J. R., Cubison, M. J., Graf, S., Lin, Y.-H., Budisulistiorini, S. H., Zhang, H., Surratt, J. D., Knochenmuss, R., Jayne, J. T., Worsnop, D. R., Jimenez, J.-L., and Canagaratna, M. R.: Ion mobility spectrometry–mass spectrometry (IMS–MS) for on- and offline analysis of atmospheric gas and aerosol species, Atmos. Meas. Tech., 9, 3245-3262, 10.5194/amt-9-3245-2016, 2016.

Le Breton, M., Wang, Y. J., Hallquist, A. M., Pathak, R. K., Zheng, J., Yang, Y. D., Shang, D. J., Glasius, M., Bannan, T. J., Liu, Q. Y., Chan, C. K., Percival, C. J., Zhu, W. F., Lou, S. R., Topping, D., Wang, Y. C., Yu, J. Z., Lu, K. D., Guo, S., Hu, M., and Hallquist, M.: Online gas-

and particle-phase measurements of organosulfates, organosulfonates and nitrooxy organosulfates in Beijing utilizing a FIGAERO ToF-CIMS, Atmos. Chem. Phys., 18, 10355-10371, 2018.

Lee, B. H., Lopez-Hilfiker, F. D., D'Ambro, E. L., Zhou, P., Boy, M., Petäjä, T., Hao, L., Virtanen, A., and Thornton, J. A.: Semi-volatile and highly oxygenated gaseous and particulate organic compounds observed above a boreal forest canopy, Atmos. Chem. Phys., 18, 11547-11562, 10.5194/acp-18-11547-2018, 2018.

Leglise, J., Muller, M., Piel, F., Otto, T., and Wisthaler, A.: Bulk Organic Aerosol Analysis by Proton-Transfer-Reaction Mass Spectrometry: An Improved Methodology for the Determination of Total Organic Mass, O:C and H:C Elemental Ratios, and the Average Molecular Formula, Anal. Chem., 91, 12619-12624, 10.1021/acs.analchem.9b02949, 2019.

Lindinger, W., Hansel, A., and Jordan, A.: Proton-transfer-reaction mass spectrometry (PTR-MS): on-line monitoring of volatile organic compounds at pptv levels, Chem. Soc. Rev., 27, 347-354, 10.1039/a827347z, 1998.

Lopez-Hilfiker, F. D., Mohr, C., Ehn, M., Rubach, F., Kleist, E., Wildt, J., Mentel, T. F., Lutz, A., Hallquist, M., Worsnop, D., and Thornton, J. A.: A novel method for online analysis of gas and particle composition: description and evaluation of a Filter Inlet for Gases and AEROsols (FIGAERO), Atmos. Meas. Tech., 7, 983-1001, 10.5194/amt-7-983-2014, 2014.

Lopez-Hilfiker, F. D., Mohr, C., Ehn, M., Rubach, F., Kleist, E., Wildt, J., Mentel, T. F., Carrasquillo, A. J., Daumit, K. E., Hunter, J. F., Kroll, J. H., Worsnop, D. R., and Thornton, J. A.: Phase partitioning and volatility of secondary organic aerosol components formed from α-pinene ozonolysis and OH oxidation: the importance of accretion products and other low volatility compounds, Atmos. Chem. Phys., 15, 7765-7776, 10.5194/acp-15-7765-2015, 2015.

Lopez-Hilfiker, F. D., Mohr, C., D'Ambro, E. L., Lutz, A., Riedel, T. P., Gaston, C. J., Iyer, S., Zhang, Z., Gold, A., Surratt, J. D., Lee, B. H., Kurten, T., Hu, W. W., Jimenez, J., Hallquist, M., and Thornton, J. A.: Molecular Composition and Volatility of Organic Aerosol in the Southeastern U.S.: Implications for IEPOX Derived SOA, Environ. Sci. Technol., 50, 2200-2209, 10.1021/acs.est.5b04769, 2016.

Lutz, A., Mohr, C., Le Breton, M., Lopez-Hilfiker, F. D., Priestley, M., Thornton, J. A., and Hallquist, M.: Gas to Particle Partitioning of Organic Acids in the Boreal Atmosphere, ACS

Earth Space Chem., 3, 1279-1287, 10.1021/acsearthspacechem.9b00041, 2019.

Mai, H., Shiraiwa, M., Flagan, R. C., and Seinfeld, J. H.: Under What Conditions Can Equilibrium Gas-Particle Partitioning Be Expected to Hold in the Atmosphere?, Environ. Sci. Technol., 49, 11485-11491, 10.1021/acs.est.5b02587, 2015.

Muller, M., Eichler, P., D'Anna, B., Tan, W., and Wisthaler, A.: Direct Sampling and Analysis of Atmospheric Particulate Organic Matter by Proton-Transfer-Reaction Mass Spectrometry, Anal. Chem., 89, 10889-10897, 10.1021/acs.analchem.7b02582, 2017.

Pagonis, D., Sekimoto, K., and de Gouw, J.: A Library of Proton-Transfer Reactions of H3O+ Ions Used for Trace Gas Detection, Journal of the American Society for Mass Spectrometry, 30, 1330-1335, 10.1007/s13361-019-02209-3, 2019.

Palm, B. B., Peng, Q. Y., Fredrickson, C. D., Lee, B., Garofalo, L. A., Pothier, M. A., Kreidenweis, S. M., Farmer, D. K., Pokhrel, R. P., Shen, Y. J., Murphy, S. M., Permar, W., Hu, L., Campos, T. L., Hall, S. R., Ullmann, K., Zhang, X., Flocke, F., Fischer, E. V., and Thornton, J. A.: Quantification of organic aerosol and brown carbon evolution in fresh wildfire plumes, Proc Natl Acad Sci U S A, 117, 29469-29477, 10.1073/pnas.2012218117, 2020.

Pankow, J. F.: An absorption-model of the gas aerosol partitioning involved in the formation of secondary organic aerosol, Atmos. Environ., 28, 189-193, 10.1016/1352-2310(94)90094-9, 1994.

Pankow, J. F. and Asher, W. E.: SIMPOL.1: a simple group contribution method for predicting vapor pressures and enthalpies of vaporization of multifunctional organic compounds, Atmos. Chem. Phys., 8, 2773-2796, 10.5194/acp-8-2773-2008, 2008.

Peng, Y., Wang, H., Wang, Q., Jing, S., An, J., Gao, Y., Huang, C., Yan, R., Dai, H., Cheng, T., Zhang, Q., Li, M., Hu, J., Shi, Z., Li, L., Lou, S., Tao, S., Hu, Q., Lu, J., and Chen, C.: Observation-based sources evolution of non-methane hydrocarbons (NMHCs) in a megacity of China, J. Environ. Sci., 124, 794-805, 10.1016/j.jes.2022.01.040, 2023.

Perraud, V., Bruns, E. A., Ezell, M. J., Johnson, S. N., Yu, Y., Alexander, M. L., Zelenyuk, A., Imre, D., Chang, W. L., Dabdub, D., Pankow, J. F., and Finlayson-Pitts, B. J.: Nonequilibrium atmospheric secondary organic aerosol formation and growth, Proc Natl Acad Sci U S A, 109, 2836-2841, 10.1073/pnas.1119909109, 2012.

685   Piel, F., Muller, M., Mikoviny, T., Pusede, S. E., and Wisthaler, A.: Airborne measurements of
686   particulate organic matter by proton-transfer-reaction mass spectrometry (PTR-MS): a pilot
687   study, Atmos. Meas. Tech., 12, 5947-5958, 10.5194/amt-12-5947-2019, 2019.

688   Piel, F., Müller, M., Winkler, K., Skytte af Sätra, J., and Wisthaler, A.: Introducing the extended
689   volatility range proton-transfer-reaction mass spectrometer (EVR PTR-MS), Atmos. Meas.
690   Tech., 14, 1355-1363, 10.5194/amt-14-1355-2021, 2021.

691   Sekimoto, K., Li, S. M., Yuan, B., Koss, A., Coggon, M., Warneke, C., and de Gouw, J.:
692   Calculation of the sensitivity of proton-transfer-reaction mass spectrometry (PTR-MS) for
693   organic trace gases using molecular properties, International Journal of Mass Spectrometry, 421,
694   71-94, 10.1016/j.ijms.2017.04.006, 2017.

695   Shiraiwa, M. and Seinfeld, J. H.: Equilibration timescale of atmospheric secondary organic
696   aerosol partitioning, Geophysical Research Letters, 39, n/a-n/a, 10.1029/2012gl054008, 2012.

697   Shiraiwa, M., Zuend, A., Bertram, A. K., and Seinfeld, J. H.: Gas-particle partitioning of
698   atmospheric aerosols: interplay of physical state, non-ideal mixing and morphology, Phys.
699   Chem. Chem. Phys., 15, 11441-11453, 10.1039/c3cp51595h, 2013.

700   Spanel, P. and Smith, D.: SIFT studies of the reactions of H3O+, NO+ and O2+ with a series
701   of alcohols, Int. J. Mass Spectrom. Ion Processes, 167-168, 375-388,
702   https://doi.org/10.1016/S0168-1176(97)00085-2, 1997.

703   Spanel, P., Ji, Y. F., and Smith, D.: SIFT studies of the reactions of H3O+, NO+ and O-2(+)
704   with a series of aldehydes and ketones, International Journal of Mass Spectrometry, 165, 25-
705   37, 10.1016/s0168-1176(97)00166-3, 1997.

706   Stark, H., Yatavelli, R. L. N., Thompson, S. L., Kang, H., Krechmer, J. E., Kimmel, J. R., Palm,
707   B. B., Hu, W. W., Hayes, P. L., Day, D. A., Campuzano-Jost, P., Canagaratna, M. R., Jayne, J.
708   T., Worsnop, D. R., and Jimenez, J. L.: Impact of Thermal Decomposition on Thermal
709   Desorption Instruments: Advantage of Thermogram Analysis for Quantifying Volatility
710   Distributions of Organic Species, Environ. Sci. Technol., 51, 8491-8500,
711   10.1021/acs.est.7b00160, 2017.

712   Tan, W., Zhu, L., Mikoviny, T., Nielsen, C. J., Wisthaler, A., Eichler, P., Muller, M., D'Anna,
713   B., Farren, N. J., Hamilton, J. F., Pettersson, J. B. C., Hallquist, M., Antonsen, S., and Stenstrom,
714   Y.: Theoretical and Experimental Study on the Reaction of tert-Butylamine with OH Radicals

in the Atmosphere, J. Phys. Chem. A, 122, 4470-4480, 10.1021/acs.jpca.8b01862, 2018.

Tani, A., Hayward, S., and Hewitta, C. N.: Measurement of monoterpenes and related compounds by proton transfer reaction-mass spectrometry (PTR-MS), International Journal of Mass Spectrometry, 223, 561-578, 10.1016/s1387-3806(02)00880-1, 2003.

Thompson, S. L., Yatavelli, R. L. N., Stark, H., Kimmel, J. R., Krechmer, J. E., Day, D. A., Hu, W., Isaacman-VanWertz, G., Yee, L., Goldstein, A. H., Khan, M. A. H., Holzinger, R., Kreisberg, N., Lopez-Hilfiker, F. D., Mohr, C., Thornton, J. A., Jayne, J. T., Canagaratna, M., Worsnop, D. R., and Jimenez, J. L.: Field intercomparison of the gas/particle partitioning of oxygenated organics during the Southern Oxidant and Aerosol Study (SOAS) in 2013, Aerosol Sci. Technol., 51, 30-56, 10.1080/02786826.2016.1254719, 2016.

Veres, P., Roberts, J. M., Warneke, C., Welsh-Bon, D., Zahniser, M., Herndon, S., Fall, R., and de Gouw, J.: Development of negative-ion proton-transfer chemical-ionization mass spectrometry (NI-PT-CIMS) for the measurement of gas-phase organic acids in the atmosphere, International Journal of Mass Spectrometry, 274, 48-55, 10.1016/j.ijms.2008.04.032, 2008.

Voliotis, A., Wang, Y., Shao, Y., Du, M., Bannan, T. J., Percival, C. J., Pandis, S. N., Alfarra, M. R., and McFiggans, G.: Exploring the composition and volatility of secondary organic aerosols in mixed anthropogenic and biogenic precursor systems, Atmos. Chem. Phys., 21, 14251-14273, 10.5194/acp-21-14251-2021, 2021.

Wang, H. L., Lou, S. R., Huang, C., Qiao, L. P., Tang, X. B., Chen, C. H., Zeng, L. M., Wang, Q., Zhou, M., Lu, S. H., and Yu, X. N.: Source Profiles of Volatile Organic Compounds from Biomass Burning in Yangtze River Delta, China, Aerosol Air Qual. Res., 14, 818-828, 10.4209/aaqr.2013.05.0174, 2014.

Wang, M. Y., Chen, D. X., Xiao, M., Ye, Q., Stolzenburg, D., Hofbauer, V., Ye, P. L., Vogel, A. L., Mauldin, R. L., Amorim, A., Baccarini, A., Baumgartner, B., Brilke, S., Dada, L., Dias, A., Duplissy, J., Finkenzeller, H., Garmash, O., He, X. C., Hoyle, C. R., Kim, C., Kvashnin, A., Lehtipalo, K., Fischer, L., Molteni, U., Petaja, T., Pospisilova, V., Quelever, L. L. J., Rissanen, M., Simon, M., Tauber, C., Tome, A., Wagner, A. C., Weitz, L., Volkamer, R., Winkler, P. M., Kirkby, J., Worsnop, D. R., Kulmala, M., Baltensperger, U., Dommen, J., El Haddad, I., and Donahue, N. M.: Photo-oxidation of Aromatic Hydrocarbons Produces Low-Volatility Organic Compounds, Environ. Sci. Technol., 54, 7911-7921, 2020a.

Wang, Q. Q., He, X., Zhou, M., Huang, D. D., Qiao, L. P., Zhu, S. H., Ma, Y. G., Wang, H. L., Li, L., Huang, C., Huang, X. H. H., Xu, W., Worsnop, D., Goldstein, A. H., Guo, H., and Yu, J. Z.: Hourly Measurements of Organic Molecular Markers in Urban Shanghai, China: Primary Organic Aerosol Source Identification and Observation of Cooking Aerosol Aging, ACS Earth Space Chem., 4, 1670-1685, 2020b.

Yatavelli, R. L. N., Lopez-Hilfiker, F., Wargo, J. D., Kimmel, J. R., Cubison, M. J., Bertram, T. H., Jimenez, J. L., Gonin, M., Worsnop, D. R., and Thornton, J. A.: A Chemical Ionization High-Resolution Time-of-Flight Mass Spectrometer Coupled to a Micro Orifice Volatilization Impactor (MOVI-HRToF-CIMS) for Analysis of Gas and Particle-Phase Organic Species, Aerosol Sci. Technol., 46, 1313-1327, 2012.

Ye, C., Yuan, B., Lin, Y., Wang, Z., Hu, W., Li, T., Chen, W., Wu, C., Wang, C., Huang, S., Qi, J., Wang, B., Wang, C., Song, W., Wang, X., Zheng, E., Krechmer, J. E., Ye, P., Zhang, Z., Wang, X., Worsnop, D. R., and Shao, M.: Chemical characterization of oxygenated organic compounds in the gas phase and particle phase using iodide CIMS with FIGAERO in urban air, Atmos. Chem. Phys., 21, 8455-8478, 10.5194/acp-21-8455-2021, 2021.

Zhang, X. and Seinfeld, J. H.: A functional group oxidation model (FGOM) for SOA formation and aging, Atmos. Chem. Phys., 13, 5907-5926, 10.5194/acp-13-5907-2013, 2013.

Zhang, X., Dalleska, N. F., Huang, D. D., Bates, K. H., Sorooshian, A., Flagan, R. C., and Seinfeld, J. H.: Time-resolved molecular characterization of organic aerosols by PILS plus UPLC/ESI-Q-TOFMS, Atmos. Environ., 130, 180-189, 10.1016/j.atmosenv.2015.08.049, 2016a.

Zhang, X., Zhang, H. F., Xu, W., Wu, X. K., Tyndall, G. S., Orlando, J. J., Jayne, J. T., Worsnop, D. R., and Canagaratna, M. R.: Molecular characterization of alkyl nitrates in atmospheric aerosols by ion mobility mass spectrometry, Atmos. Meas. Tech., 12, 5535-5545, 10.5194/amt-12-5535-2019, 2019.

Zhang, X., Krechmer, J. E., Groessl, M., Xu, W., Graf, S., Cubison, M., Jayne, J. T., Jimenez, J. L., Worsnop, D. R., and Canagaratna, M. R.: A novel framework for molecular characterization of atmospherically relevant organic compounds based on collision cross section and mass-to-charge ratio, Atmos. Chem. Phys., 16, 12945-12959, 10.5194/acp-16-12945-2016, 2016b.

775   Zhao, Y. L., Kreisberg, N. M., Worton, D. R., Isaacman, G., Weber, R. J., Liu, S., Day, D. A.,
776   Russell, L. M., Markovic, M. Z., VandenBoer, T. C., Murphy, J. G., Hering, S. V., and Goldstein,
777   A. H.: Insights into Secondary Organic Aerosol Formation Mechanisms from Measured
778   Gas/Particle Partitioning of Specific Organic Tracer Compounds, Environ. Sci. Technol., 47,
779   3781-3787, 2013.

780   Zhu, H., Wang, H., Jing, S., Wang, Y., Cheng, T., Tao, S., Lou, S., Qiao, L., Li, L., and Chen,
781   J.: Characteristics and sources of atmospheric volatile organic compounds (VOCs) along the
782   mid-lower Yangtze River in China, Atmos. Environ., 190, 232-240,
783   10.1016/j.atmosenv.2018.07.026, 2018.

784   Zhu, S., Wang, Q., Qiao, L., Zhou, M., Wang, S., Lou, S., Huang, D., Wang, Q., Jing, S., Wang,
785   H., Chen, C., Huang, C., and Yu, J. Z.: Tracer-based characterization of source variations of
786   PM2.5 and organic carbon in Shanghai influenced by the COVID-19 lockdown, Faraday
787   Discuss, 226, 112-137, 10.1039/d0fd00091d, 2021.

788

789
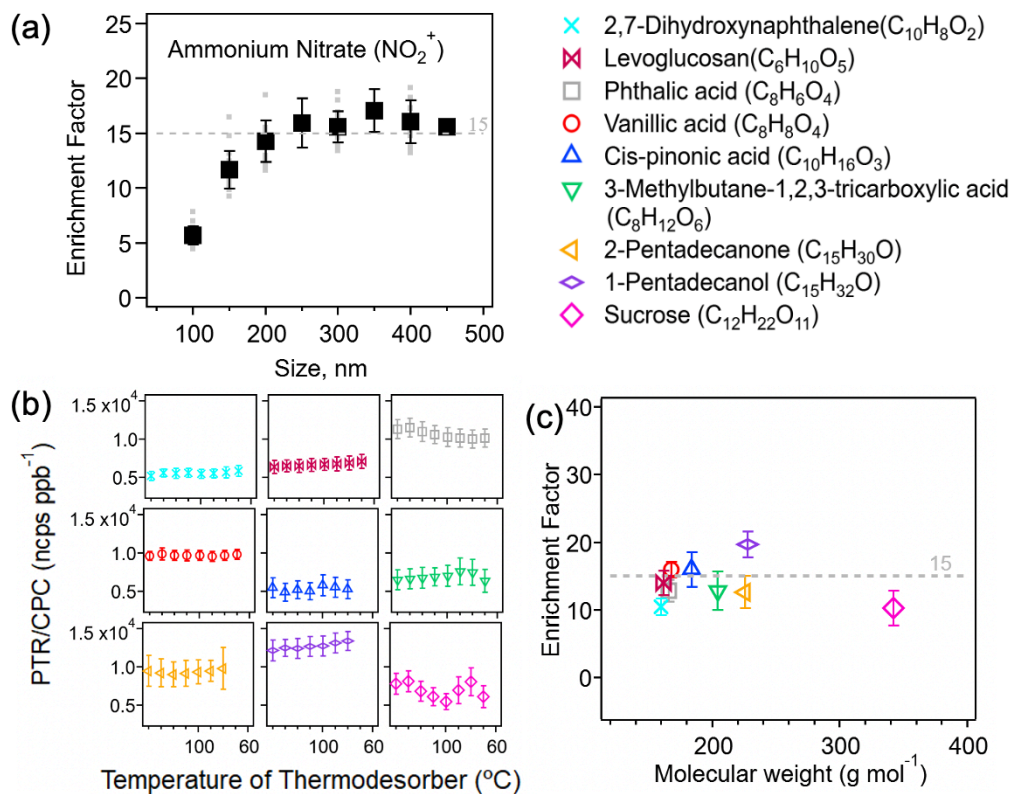
790

791 Figure 1. (a) Measured unitless enrichment factor (*EF*) of ammonium nitrate particles as a

792 function of particle size in the 100 – 450 nm range. Grey markers represent all replicating

793 measurements. The error bar denotes one standard deviation (1σ) of the average. (b) Ratios of

794 PTR-ToF-MS signals (including both parent and fragment ions) to CPC counts (±1σ) at 300

795 nm for all organic standards studied. (c) *EF* (±1σ) of selected organic standards based on the

796 calculated sensitivity.

797
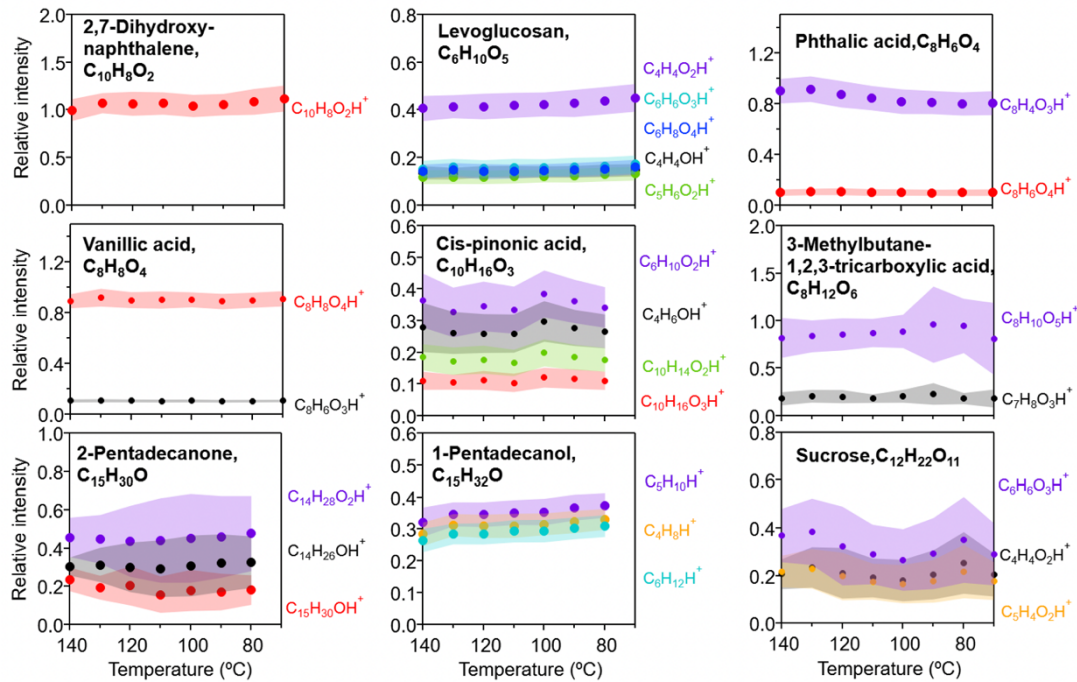
798

799 Figure 2. Ratios of CHARON-PTR-ToF-MS signals (ncps) to CPC measurements (ppb) of all

800 detected ions (including both parents and fragments) for a given pure organic standard tested

801 under different desorption temperatures (70 – 140 °C), normalized to the corresponding ratios

802 obtained at 140 °C. Ions with relative intensities less than 10% are excluded. Red markers

803 represent the parent peaks. Colored shades represent the relative standard deviations at different

804 temperatures (exact values are given in Table S4).

805
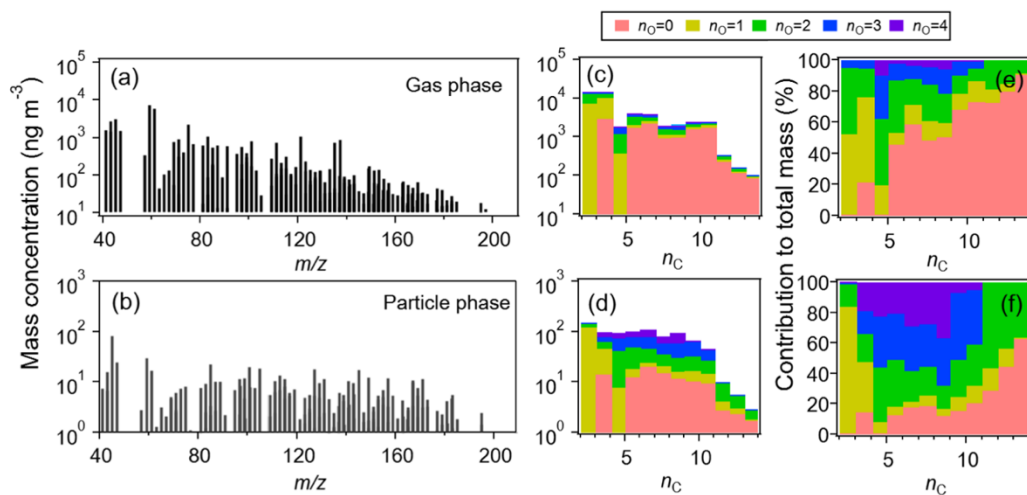
806

807 Figure 3. Background subtracted monthly-average PTR-ToF-MS mass spectra in the (a) gas

808 phase and (b) particle phase. Mass distributions of all identified species resolved by the carbon

809 and oxygen numbers (n_C and n_O) in the (c) gas phase and (d) particle phase, as well as their

810 relative contribution to the total organic mass in the (e) gas phase and (f) particle phase.

811
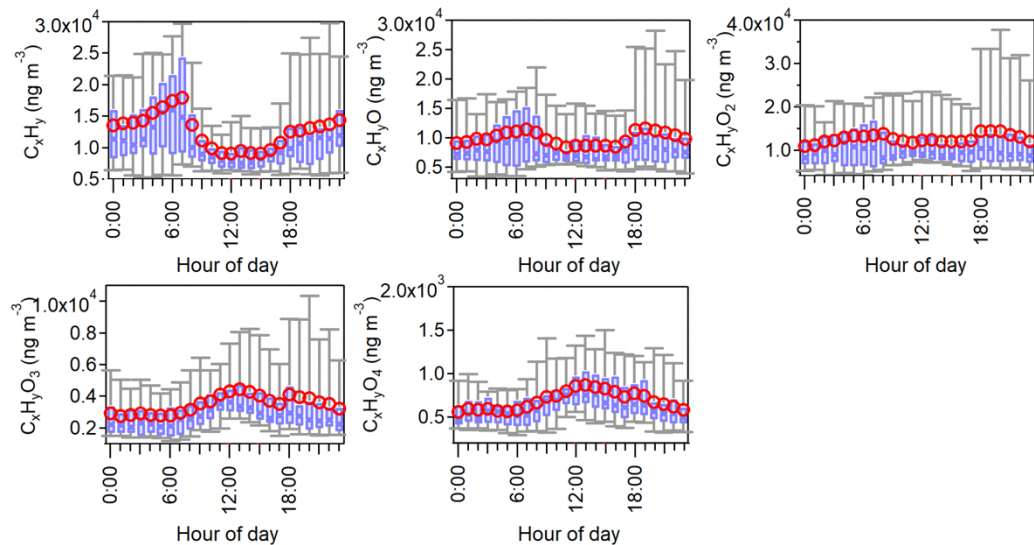
812

813 Figure 4. Diurnal variations of observed gas-phase species with a generic formula of $C_{2-13}H_{2-22}O_{0-4}$. Hourly average values (ng m^{-3}), together with 10th, 25th, 75th, and 90th percentiles, are

815 also plotted.

816
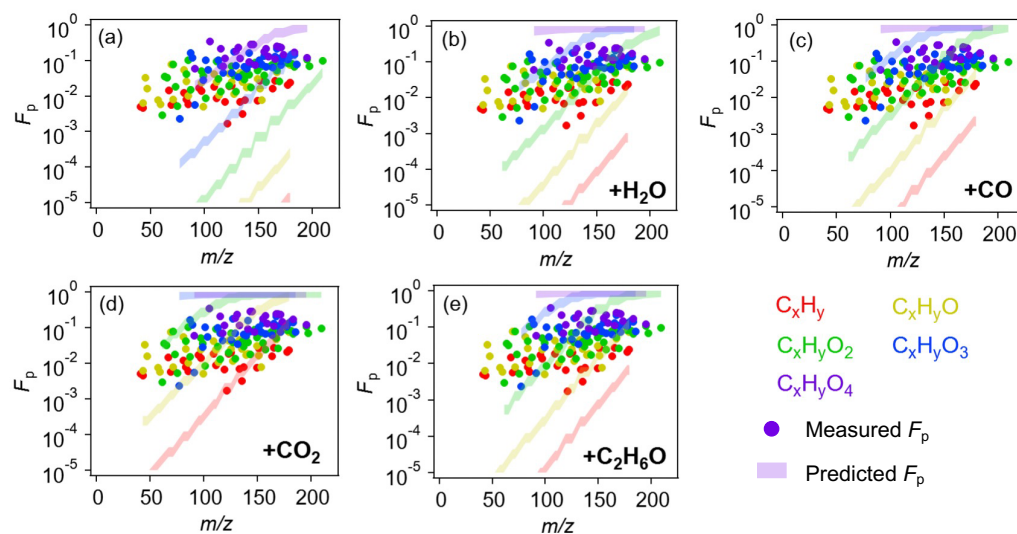
817

818 Figure 5. (a) Campaign average fraction of organic species in the particle phase (F_p) grouped

819 by the oxygen number. Solid markers represent the calculated F_p based on the CHARON-PTR-

820 ToF-MS measurements. Colored shades represent the predicted F_p of corresponding molecular

821 formulas. (b-e) Measured vs. predicted F_p assuming the identified species are fragments of

822 corresponding parent compounds through neutral losses of H_2O, CO, CO_2, and C_2H_6O,

823 respectively (values are given in Table S5).

824